A framework for machine-learning-augmented multiscale atomistic simulations on parallel supercomputers

Marco Caccin [*], Zhenwei Li [†*], James R. Kermode [‡*], Alessandro De Vita [*§]

April 3, 2015

Abstract

Recent advances in quantum mechanical(QM)-based molecular dynamics simulations have used machine-learning (ML) to predict, rather than re-calculate, QM-accurate forces in atomic configurations sufficiently similar to previously encountered ones. Here, we discuss how ML approaches can be deployed within large-scale QM/MM materials simulations on massively parallel supercomputers, making QM zones of $\gtrsim$ 1000 atoms routinely attainable. We argue that the ML approach allows computational effort to be concentrated on the most chemically active subregions of the QM zone, significantly improving the overall efficiency of the simulation. We thus propose a novel method to partition large QM regions into multiple subregions which can be computed in parallel to achieve optimal scaling. Then we review a recently proposed QM/ML MD scheme [Z. Li et al., Phys. Rev. Lett. 114(9), 096405 (2015)], discussing how this could be efficiently combined with QM-zone partitioning.

[*]King's College London, Department of Physics, Strand, London WC2R 2LS, United Kingdom

[†]Department of Chemistry, University of Basel, Klingelbergstrasse 80, CH-4056 Basel, Switzerland

[‡]Warwick Centre for Predictive Modelling, School of Engineering, University of Warwick, Coventry CV4 7AL, United Kingdom

[§]CENMAT-UTS, Via Alfonso Valerio 2, 34127 Trieste, Italy

INTRODUCTION

Many processes in nature involve the concerted action of phenomena taking place across different length scales, so that simulating them requires large model systems and is best achieved by adopting a non-uniform precision atomistic approach. An archetype of such problems is the chemomechanical behaviour of a brittle material, in which the macroscopic mechanical stress field in a material is bidirectionally coupled with atomic-scale chemical reactions.[1] Consider e.g., the stress-corrosion cracking of silica in the presence of water: molecules in the proximity of the crack tip as well as those in pores within the material are known to modify the stress field in the solid, which in turn determines the local atomic strain that influences the bond breaking reactions and diffusivity of water into the material.[2] A quantum mechanically accurate method based on density functional theory (DFT) is necessary here to capture the details of water dissociation, bond breaking mechanisms and to accurately model highly strained bonds concentrated near the crack tip.[3] An interatomic potential is instead sufficient to describe the remainder of the system — typically requiring $\sim 10^6$ atoms to accommodate large stress gradients — where less complex chemistry is involved. An even more complex system is the propagation of a crack front in hydrogen embrittled steels.[4] While little is known on the exact modalities of this intriguing phenomenon, it is clear that brittle fracture propagation steps and dislocation loop emission at localised crack front regions will both take place. As in the example above, here too bond breaking phenomena involving complex chemistry are bound to locally occur within subportions of the overall chemically active region, although the exact locations will not be predictable *a priori*. The nature of these systems has a direct bearing on how an efficient molecular dynamics scheme to simulate them should be constructed.

To begin with, despite Moore's law a monolithic full-DFT description of the entire system remains hopelessly out of reach. A multiscale QM/MM approach is thus *necessary* to address these kinds of 'chemomechanical' situations where both local chemistry and long-range stress fields must be modelled. For this reason, computationally efficient multiscale coupled QM/MM methods[5] have been developed, where DFT is only used where necessary (close to a moving crack tip or a dislocation in the examples above). However, the regions requir-

ing quantum mechanical treatment may still contain thousands of atoms when adopting a multiscale approach, and ordinary cubic scaling $\mathcal{O}(N^3)$ plane-wave DFT packages[6,7] cannot effectively be used.

While some benefits may be gained by using $O(N)$ QM approaches, recent advances have pointed to new ways of speeding up QM-based simulations.[8–11] Namely, it has become clear that a new class of informationally efficient Machine Learning (ML) algorithms could 'remember/interpolate', rather than recalculate, previously seen QM information e.g., energy or forces for a given atomic configuration. In an ideal learning approach, fresh QM information needs to be computed only if anything genuinely 'new' happens along the trajectory. Such new events could, however, be limited to localised zones e.g., the crack front point where a dislocation loop emission initiates. QM calculations should then be limited to these regions, which are typically much smaller than the full QM zone. These regions will also very likely be smaller than the typical system sizes beyond which $O(N)$ QM techniques[12,13] become faster than $O(N^3)$ approaches, so using an overall QM/MM scheme constrained to use a single $O(N)$ calculation for the full QM zone is not an optimal choice. The considerations above instead suggest that an optimal algorithm could involve carrying out an embarrassingly parallel (and possibly easily load-balanced) swarm of localised QM calculations on system subregions, somehow 'importance sampled' to develop novel information just where and when it is necessary. It should be noted upfront that renouncing the idea of carrying out a single QM calculation will invariably deny the possibility of strictly enforcing energy conservation (null work over any closed loop), as the forces made available to the dynamics will not be derived from a unique and well-defined Hamiltonian. However, it is important to realise that energy conservation must in all cases be renounced as soon as there is a dynamically evolving QM zone containing different atoms at different simulated times.[5,14] Thus, while accurate forces will be made available by QM/MM algorithms, the absence of a mathematically conserved total energy is unavoidable in most situations of interest.

Constructing a practical scheme along the lines sketched above requires merging two key components, both discussed in the remainder of this work. The first one is a scheme capable of subdividing the full QM zone (or any large connected portion of it) into a number of smaller and more manageable subparts, still large enough so that the QM engine in

use remains efficient on a large number of computer cores e.g., $\sim$ 1000 cores for a $O(N^3)$ code on current HPC architectures. This will be discussed in the next section, where we introduce an ensemble parallel framework algorithm for QM zone subdivision. The second component is an efficient implementation of the learning/remembering strategy anticipated above. This must typically include a database of local configurations for which QM forces are known, an inference scheme to predict forces in new situations, and a rationale for deciding when it is preferable to calculate QM forces rather than trying to predict them. A suitable implementation will be addressed in the successive section, where we describe a recently proposed ML-based MD scheme,[10] based on Bayesian inference carried out by means of Gaussian process regression. Possible ways in which these two technical developments could be merged into an accurate and efficient QM-based MD scheme suitable for HPC are discussed in the final Outlook section.

ENSEMBLE PARALLEL FRAMEWORK

Ensemble LOTF

We have developed a new framework building on the existing QM/MM 'Learn On The Fly' (LOTF)[14,15] implemented in the libAtoms/QUIP code.[16] The code supports classical molecular dynamics (MD) with a wide range of interatomic potentials including the machine learning based Gaussian Approximation Potentials (GAP)[9], while the QM calculations are carried out with widely used DFT packages.[6,7,17] One or more QM regions are typically identified and tracked along the trajectory using problem-based criteria e.g., atomic coordination, local atomic strain or chemical composition. Within the LOTF method, a universal two-body potential is added to the underlying interatomic potential and fitted to match target forces computed in the QM region every few timesteps, and the trajectory of the whole system is evolved according to the QM-informed global potential in a predictor-corrector fashion.[14] At the boundaries between QM and MM regions, the two levels of representation are seamlessly coupled by a force mixing method that enforces momentum conservation and matching of lattice parameters and elastic constants.[5] Based on the concept of near-sightedness of quan-

tum mechanics,[18] the correct forces acting on the atoms of a 'core' QM region $\mathcal{C}$ can be obtained by carrying out calculations on a subsystem carved out of the complete system: this comprises $\mathcal{C}$ and a portion of the surrounding atomic environment, denoted as 'buffer' QM region $\mathcal{B}$. From now on we will denote a set of atoms with calligraphic letters (e.g., $\mathcal{C}$), and the number of atoms contained in it with the cardinality notation (e.g., $|\mathcal{C}|$). The buffer $\mathcal{B}$ surrounding $\mathcal{C}$ ensures that all atoms in $\mathcal{C}$ have a fully QM-represented local environment, which removes the risk of introducing large force errors due to spurious surface effects. The thickness of the buffer region is system-dependent, and is typically in the range of 5–10 Å.[5,19] Similar to previous QM/MM approaches, when dealing with non-metallic systems, it is often found that $|\mathcal{B}|$ can be significantly reduced by appropriate saturation of the unphysically cut 'dangling' bonds, usually by means of artificially introduced hydrogen atoms.

The LOTF framework outlined above has been successfully adopted to investigate a range of physical problems in semiconductors, such as point defect diffusion,[14] impurity-driven scattering mechanisms in propagating cracks[20], and stress-corrosion cracking.[21,22] More complex systems such as oxides and amorphous materials — of which amorphous silica is a prominent example — or transition metal systems such as hydrogen-containing steels are associated with a significantly higher computational cost, either because larger buffer regions are needed to accurately describe longer-range interactions[19] or simply as a result of the increased number or valence electrons per atom. As a result, there is a strong case for seeking further efficiency improvements to enable hundreds of picoseconds-long QM/MM dynamics with thousands of DFT atoms on current state-of-the-art supercomputing facilities.

Taking advantage of the fact that in the LOTF scheme the coupling between the QM and MM regions is mediated by forces only — which are locally-defined quantum-mechanical observables, in contrast to global quantities such as energy — in this work we propose splitting the (not necessarily connected) QM region into k subdomains and extracting the correct QM forces from k independent concurrent DFT calculations performed on each subdomain. In HPC architectures (e.g., IBM Blue Gene/Q), a given number of compute nodes (CNs) N_{tot} can be partitioned into N_{blocks} blocks of size $N_{\mathrm{CN}} = N_{\mathrm{tot}}/N_{\mathrm{blocks}}$ in order to run multiple simultaneous tasks on separate CN subsets (we assume for simplicity that all blocks have the same size). Allowed partition sizes are often restricted to powers of two, so

$N_{\mathrm{tot}}, N_{\mathrm{blocks}}, N_{\mathrm{CN}} \in \{2^N \mid N \in \mathbb{N}\}$. DFT force evaluation is the rate-limiting part of these simulations, so only one block needs to be assigned to the classical dynamics operations and all the remaining $k = 2^N - 1$ blocks can be assigned to independent DFT tasks. In doing so, the number of QM zone subdomains k and the number of compute nodes N_{CN} allocated to each subdomain act as tuneable parameters that allow running any chosen DFT engine on its closest-to-optimal number of CNs for the typical size of the QM cluster to be evaluated, thus minimising overall use of computational resources. Furthermore, this also enables optimal tiling of the allocated processors across different executables. As exemplified in Fig. 1, if we carried out a single DFT calculation for the whole QM zone either (a) a significant number of the available processors would be left unused or (b) the MM code would have to run on an unnecessarily large number of cores, while the ensemble parallel scheme (c) guarantees that all resources are optimally used.

To connect the QUIP MM and DFT runs we have implemented a socket-based communication protocol, which is mediated via a lightweight Python script running on the front-end node (FEN). Using standard UNIX sockets has the advantage of being relatively architecture independent. The source code for our implementation of this server and a number of clients including both MM and QM packages is available online.[23]

QM region partitioning

Since QM forces are only needed at every QM step of the LOTF algorithm (i.e. only once for every predictor/corrector cycle, that is every ~ 10 MD steps in typical applications), it is crucial to maximise the load balance between the concurrent DFT calculations. The wall-clock time to solution for a DFT electronic structure minimisation in a chemically uniform system is, to a first approximation, an increasing function of the number of atoms: in an ensemble of DFT calculations it is determined by the total number of atoms (sum of atoms in core and buffer) associated with the largest QM cluster. Since the construction of a buffer and its bond termination follow a complex set of heuristic rules, this total number is not exactly predictable, and the best strategy is (i) to split $\mathcal{C}$ into k subdomains $\mathcal{C}_i\,, i = 1, 2, \ldots, k$ containing an approximately equal number of atoms and (ii) make the subdomains $\mathcal{C}_i$ as convex as possible. While the first requirement takes care of load balancing, the second is

essential to reduce the total number of atoms $|\mathcal{C}_i \cup \mathcal{B}_i|$ in each cluster: the smaller the aspect ratio of $\mathcal{C}_i$ is, the smaller the ratio between core and buffer atoms will be. By drawing an analogy between a set of bonded atoms and an undirected graph, the problem of splitting $\mathcal{C}$ can be recast as a graph partitioning problem. Given a set of n atoms (graph vertices set V) linked by a set of chemical bonds (graph edges set E), we wish to divide the corresponding graph $G(V, E)$ into k subgraphs comprising approximately the same number n/k of vertices, so that some appropriate measure of the spatial convexity of each part is maximised under the constraint that each subgraph be connected. This problem belongs to the class of k-way graph partitioning problems (k-GPP), for which practical solutions are found by means of approximate methods such as the Kernighan-Lin algorithm,[24] Fiduccia-Mattheyses algorithm,[25] spectral partitioning,[26,27] and multi-level algorithms.[28] Our proposed k-way partitioning algorithm comprises three steps: (i) identification of connected components, (ii) a rough initial partitioning via standard methods and (iii) a problem-specific refinement step. Initially, each of the internally connected parts $G^{(j)}$ of the whole graph G (such as a molecule or a spatially separate cluster of atoms) is identified by a shortest path length search over each vertex.[29] For a given total number k of partitions, each part $G^{(j)}$ containing $n^{(j)}$ vertices will be divided in approximately $k^{(j)} = k\, n^{(j)}/n$ subgraphs, with the further constraint that $\sum k^{(j)} = k$. Each $G^{(j)}$ is then treated independently.

In the current implementation, the initial partitioning can be performed via known methods, such as the k-medoids algorithm,[30] iterative spectral bisection,[26,31,32] or more elaborate methods such as those included in the METIS package.[28] For a given connected graph $G^{(j)}$, the result of this operation is a set of connected subgraphs $\{S_i^{(j)}\}_{i=1,\ldots,k^{(j)}}$ and a set of cut edges E_{cut} so that

$$\left(\bigcup_i S_i^{(j)} \right) \cup E_{\text{cut}} = G^{(j)}. \tag{1}$$

Subsequently, for the refinement step we can think of the subgraphs obtained as a set of neighbouring grains that compose the original graph $G^{(j)}$. As in the case of inverse Ostwald ripening, of which digestive ripening of nanoparticles is a well-known example,[33] we wish to obtain a monodisperse set of grains while still minimising the overall dimension of the grain boundaries. Ostwald ripening is a thermodynamically driven process, and as such applying

it to our problem requires the definition of a free energy-like quantity for the graph, along with a surface energy and a grain diameter. From the list of edges of the initial graph $G^{(j)}$ it is straightforward to calculate the bond-hopping distance matrix $D(G^{(j)})$ by a breadth-first search algorithm, and from it the distance matrix of each subgraph $D(S_i^{(j)})$ by extracting the relevant rows and columns. Dropping the superscript (j) for the sake of clarity, the cost function

$$F(S_i) = \sum_{a,b} \left(D_{a,b}\left(S_i\right)\right)^2 \tag{2}$$

is a property of subgraph $S_i \subseteq G$ which is related to both its number of vertices and the convexity of its corresponding atomic cluster. For instance, given a fixed number of vertices the value of F increases as the aspect ratio of the cluster increases because so does the average distance between atoms (measured by either bond-hopping or by a Euclidean metric). For a fixed aspect ratio, F will also increase with the number of vertices because the summation includes more elements, while statistically the average distance between pairs of vertices (atoms) a, b will also increase. Based on this rationale, we can devise an algorithm that minimises the global cost function

$$F(G) = \sum_i F(S_i) \tag{3}$$

by swapping vertices from subgraphs with high cost function to others with lower values, using F as the driving force for optimising shape and equalising size across subgraphs. The proposed digestive ripening algorithm is the following:

1. Provide an initial guess $\{S_1(V_1, E_1), \ldots, S_k(V_k, E_k)\}$ for the k-way partitioning of the connected graph $G(V, E)$.

2. Calculate all cost functions $\{F(S_i)\}$ and sort them in decreasing order of absolute difference from the average value. Store indices of sorting order I and pick the first entry $i^* \in I$.

3. Look for a vertex swap for S_{i^*}:

   - Get the list $E_{i^*}^{\text{neigh}} \subseteq E$ of boundary edges connecting S_{i^*} with its neighbour sub-graphs:

$$(v_a, v_b) \in E_{i^*}^{\text{neigh}} \Leftrightarrow v_a \in V_{i^*} \wedge v_b \in V_j \,, i^* \neq j \tag{4}$$

- For every edge in $E_{i^*}^{\mathrm{neigh}}$ try to assign both end vertices a, b to the subgraph with the lowest cost function. Discard the move if it produces a null graph, otherwise calculate the free energy variation

$$\Delta = F(S_{i^*}^{\mathrm{new}}) + F(S_j^{\mathrm{new}}) - F(S_{i^*}^{\mathrm{old}}) - F(S_j^{\mathrm{old}}) \tag{5}$$

  and store the move if $\Delta < 0$

- If it exists, apply the highest-gain (lowest Δ) move among those that preserve the connectedness of the donor subgraph and go to (2), otherwise choose next $i^* \in I$ and go to (3)

4. Exit if no further favourable move is found.

The algorithm is parameter-free (except for the desired target number of partitions k), deterministic for a given initial partitioning guess. We note, however, that generalisation to simulated annealing searches are straightforward, once the strict cost function descent constraint is lifted. It also works seamlessly with periodic boundary conditions and, similarly to other common techniques,[25] applies only one swapping operation at a time which guarantees connected subgraphs at all stages. Fig. 2 illustrates a step of the digestive ripening process for a small example graph.

QM region update

After the partitioning and on the basis of the obtained subgraphs $S_i^{(j)}$, each core QM subregion is carved out of the whole system, and buffer atoms bond terminations are then added as previously explained, to guarantee convergence of core atom forces as already discussed. We note that isolated "outlier" clusters whose sizes are significantly higher than average can occur at this stage, although in our experience the procedure outlined in the previous section is sufficiently effective to drastically limit their number. These can be treated with a trivial modification of the partitioning scheme outlined above, where the partitioning loop is run using a slightly lower initial $\hat{k} = k - k_{res}$ target number of subdomains, keeping k_{res} blocks "in reserve" to split in two smaller subdomain units the QM subdomains associated with

the k_{res} largest clusters. The resulting swarm of k atomic clusters $\mathcal{C}_i \cup \mathcal{B}_i$ can at this point be simultaneously sent for calculation.

As an MD simulation progresses, the QM region is automatically tracked and selected, and only every so often is the difference between two QM regions of subsequent timesteps (from now on designated as 'old' and 'new') sufficient to justify the execution of an *ex novo* partitioning and buffering. Avoiding such operations when they are not necessary increases the continuity of the QM clusters along the system trajectory, so that when possible we assign the same set of atoms to the same set of processors. This is important for efficiency, since whenever a new QM cluster is 'similar enough' to the old one, the wavefunctions and electron density already present in memory can be used as the starting point for a continuation run, which can significantly reduce the time to solution. To decide whether or not updating the partitioning of the QM region $\mathcal{C}$, similarity criteria are first applied to it as a whole: if neither the set of atoms in $\mathcal{C}$ nor the list of atomic bonds in $\mathcal{C} \cup \mathcal{B}$ has changed, a new partitioning and cluster carving procedure is avoided and the previous k QM clusters may be reused. In this case the atomic positions of the old QM clusters are simply updated in place, and we additionally check each new buffered cluster for compatibility with its previous state through a checklist: (i) the set of atoms $\mathcal{C}_i \cup \mathcal{B}_i$ has not changed, (ii) the lattice vectors have not changed (only meaningful if clusters are periodic along any direction), (iii) the mean squared displacement of atomic positions between new and old cluster is less than a given threshold that depends on the QM engine in use. If for a given cluster all these criteria are met, the setup already present in memory is suitable for a continuation of the previous QM calculation.

Results: performance of the ensemble parallel scheme

In the following we present the results of tests performed on the *Mira* IBM Blue Gene/Q (BG/Q) machine located at the Argonne Leadership Computing Facility. Each BG/Q compute node is a PowerPC A2 1600MHz processor containing 16 cores capable of 4-way hyperthreading.[34] We used the plane-wave DFT package VASP 5.3,[6] which is parallelised via MPI only and thus allows up to 16 processes per compute node. Electronic exchange and correlation were described using the PBE functional throughout this section.

The QM calculation step is by far the most computationally expensive step of any QM/MM approach. We will thus concentrate on the performance of our novel ensemble DFT scheme for QM/MM calculations, which is largely determined by the quality of the multi-step partitioning algorithm we developed, and can be measured in terms of the total computational cost and time to solution (t.t.s.) of a DFT force evaluation for a given core QM region $\mathcal{C}$ contained in a larger system. The tuneable parameters of the scheme are (i) the number of CNs assigned to each DFT instance N_{CN} and (ii) the number k of partitions in which to divide $\mathcal{C}$. The parameters that intrinsically depend on the system under investigation are (i) the total number of core atoms $|\mathcal{C}|$ and their geometry, and (ii) the buffer size necessary to obtain converged QM forces for a given core QM region.

We first test the scaling properties of our DFT package of choice to identify the optimal combination of atomic cluster size $|\mathcal{C} \cup \mathcal{B}|$ and N_{CN} compatible with the computing architecture in use. In the limit of a perfectly linear scaling DFT code and vanishing buffer region, there would be evidently no need to split $\mathcal{C}$ and the best choice would be to run a single calculation on all the available CNs; in other scenarios, however, dividing the problem is likely to be advantageous. Based upon the computed benchmarks, we fixed $N_{CN} = 64$ nodes (equivalent to 1024 compute cores) and tune k to produce individual QM clusters with sizes $|\mathcal{C} \cup \mathcal{B}| \sim 300$ atoms. According to the optimal tiling requirements previously illustrated, we set the number of partitions to $k = 2^N - 1$ for some integer N. To investigate the weak scaling properties of our method we choose a physical system of real interest: a configuration of atoms in the neighbourhood of a crack tip in amorphous silica (a-SiO_2) under tensile load, illustrated in Fig. 3. Periodic boundary conditions (PBC) are applied along the crack front direction (z) with periodicity 30 Å, providing suitable boundary conditions for the crack slab while still reproducing well the radial distribution function of the real amorphous (hence non-periodic) material. The region $\mathcal{C}$, shown in red in Fig. 3b, is the minimal QM core region necessary to obtain an accurate description of bond rupture and crack propagation in the modelled material. Due to long-range electrostatic interactions in the system, the buffer region is significantly larger than this relatively small core region. The partitioning of $\mathcal{C}$ is performed in 3 steps: (i) iterative spectral bisectioning; (ii) merging of the two smallest neighbouring subgraphs to obtain $2^N - 1$ parts; (iii) digestive ripening to equalise the sizes

and optimise the shapes of $\mathcal{C}_i$.

A weak scaling benchmark needs a set of tasks of increasing problem size to which proportionally increasing computing capability are allocated. In our system a useful definition of problem size is the number of accurate DFT forces required in region $\mathcal{C}$, which is equal to the number of atoms $|\mathcal{C}|$; the computing capability is the total number of CNs of the ensemble QM/MM calculation. We can obtain different problem sizes by replicating the system along z and keeping the ratio $|\mathcal{C}|/k$ constant. The presence of surfaces in the system makes the buffer sizes $|\mathcal{B}_i|$ less predictable, but with this choice the ratio between surface and bulk atoms is kept constant. A scenario in which replication of the system along the z axis is necessary is, for instance, the study of quasi-3D crack fronts. Fig. 4 shows, for a cluster $\mathcal{C}_i \cup \mathcal{B}_i$, the correlation between the cost function $F(\mathcal{C}_i)$, which is the variable driving the partitioning process, and the computational cost of the DFT calculation of the cluster $\mathcal{C}_i \cup \mathcal{B}_i$, which we can assume to be a monotonically increasing function of the number of valence electrons. For the reasons already mentioned (e.g., presence of surface atoms, complex buffering and bond termination heuristics), perfect correlation is not to be expected, but F is nevertheless a representative quantity which is meaningful to equalise across subgraphs.

The timing results for t.t.s. for a single-point DFT calculation is shown in Fig. 5 for the case of continuation calculations in which the in-place update of all clusters $\mathcal{C}_i \cup \mathcal{B}_i$ has occurred. In our method the time to calculate all forces in $\mathcal{C}$ is the maximum t.t.s. encountered while concurrently carrying out all the k DFT calculations on the separate clusters. The overall good scaling of the ensemble method is easily explained once we note that the generated clusters have about the same number of atoms, regardless of the total problem size $|\mathcal{C}|$. Moreover, moving to larger systems at the same time as increasing k can reduce the overall t.t.s., both by producing better cluster size distributions and by the progressively lessening effect of the presence of one computing block assigned to the classical dynamics. The minimum size of the test system containing a complete crack front as in Fig. 3b contains $|\mathcal{C}| = 218$ atoms, which in a non-ensemble framework would result in a single large cluster (periodic along z) of $|\mathcal{C} \cup \mathcal{B}| \sim 1300$ atoms for which a plane-wave DFT code is no longer a viable choice. For a comparison with the current state-of-the-art codes, we show the timings obtained with CP2K[17] on one large cluster with equivalent DFT accuracy

parameters. CP2K allows hybrid MPI/openMP parallelism, thus making full use of all the available 64 threads per compute node. While the t.t.s. of the two methods are comparable for sufficiently small system sizes, the advantage of splitting the workload across independent executables becomes evident. It should also be noted that the overall computational cost of carrying out a single DFT calculation would be in real terms actually almost double that shown as red triangles in Fig. 5, due to tiling inefficiency of the kind depicted in Fig. 1a, not incurred in the ensemble approach. Furthermore, our ensemble framework is not tied to a specific DFT code: it can be then envisioned that choosing the best performing code for a given machine architecture would lower the t.t.s. of each parallel calculation while at the same time keeping the scaling trend intact.

We next analyse the strong scaling of our method, i.e. the speedup when tackling a fixed size problem with increasing computing resources. A minimal realistic crack front in a-SiO_2 is too large a system to be investigated by a single plane-wave DFT calculation, so for these tests we instead studied a crack front in crystalline Si comprising $|\mathcal{C}| = 111$ core QM atoms. Moreover, the covalent nature of the bonding leads to shorter-range interactions, so the buffer regions required are much smaller.[19] As can be observed in Fig. 6, a single plane-wave DFT code cannot efficiently make use of the increasingly available computational power; conversely, excellent strong scaling can be obtained when the task is split among several independent instances of the same DFT executable. By means of this test, for the given system and DFT engine we can set the variable k so that the overall computational cost is minimised (here obtained for $k = 7$).

MACHINE LEARNING MOLECULAR DYNAMICS

We next briefly review a ML MD scheme targeted at efficiently harnessing the stream of QM data flowing from CPU-intensive first principles calculations like those described above. A way to combine the ensemble parallelism approach with this scheme, with the potential of significantly enhancing the usefulness of both techniques in large scale simulations, will be discussed in the Outlook section below. Rather than attempting to build up a full picture of the QM potential energy surface (PES) as has been done before, notably using neural

networks[8] or Gaussian Process (GP) regression,[9] our approach focusses on learning the QM *force* acting on an atom given its local environment. We use GP regression[35] to infer the most probable QM force on a new atomic environment given a database of previous observations and a Gaussian prior distribution expressed via a smooth covariance kernel. Direct force learning circumvents the numerical errors associated with the differentiation of a PES constructed on the ML teaching set points for the evaluation of forces in energy-based ML schemes. Moreover, a force-learning scheme enables us to add novel information to the teaching database 'on-the-fly', with the QM engine being called only if the information within the existing database is insufficient to infer QM forces on a configuration of interest. In this way, the force accuracy can be kept closely in line with that of the QM target. For simple test systems we find that the training data becomes essentially complete after a limited initial training period, after which the predicted ML forces are sufficient to accurately determine the further trajectory evolution. For more complex systems the rate at which new data needs to be learnt systematically decreases as the phase space of the system already explored increases, and intensive learning only takes place where novel chemical complexity is encountered. As a further appealing feature of ML methods, large-scale teaching datasets can be generated by combining data from any compatible set of calculations, and results from separate simulations across different projects can be integrated in one progressively growing knowledge pool.

Learning Forces From Atomic Environments

Given an atom, its local atomic environment is defined as the set of neighbouring atoms within a prescribed cutoff radius. For covalent materials, such as Si, considering only the ~ 100 neighbouring atoms within 8 Å is sufficient to converge DFT forces to an accuracy of 0.05 eV/Å, which is comparable with the typical accuracy of forces in a DFT calculation. For systems where long range electrostatic forces are important, such as oxides, we envisage that a global classical Coulomb model based on fixed multipole moments could be added to the ML-predicted short-ranged forces to produce a faithful model of the overall interactions. Developing a representation for atomic environments that is appropriate for learning QM forces is a notable challenge of this approach. To reduce the dimensionality of the GP

regression problem, the representation should possess the intrinsic symmetries of the force, and thus be invariant under rigid rotation, translation, inversion as well as any permutation of atoms of the same chemical species. As a first approach, we have proposed a simple vector description of the local environment around an atom consisting of a set $\{\mathbf{V}_i\}$ of n_{IV} internal vectors (IVs) which, by construction, encode the relevant symmetries of the QM force vector. A set of IVs can be defined using the formula

$$\mathbf{V}_i = \sum_{q=1}^{N_{\mathrm{neighb}}} \hat{\mathbf{r}}_q \, \exp\left[-\left(\frac{r_q}{r_{\mathrm{cut}}(i)} \right)^{p(i)} \right] . \tag{6}$$

This set can be augmented by additional vectors such as forces derived from relevant simpler interaction models, e.g., the Stillinger-Weber interatomic potential[36] in the case of Si or the Tangney-Scandolo linear scaling polarisable interatomic potential in the case of a-SiO_2 system.[37] Testing reveals that such augmentation can significantly improve force prediction accuracy, suggesting that simpler force fields — while not necessarily accurate enough to be used on a standalone basis — encode useful information which can be exploited by learning the correlation of the forces they predict with the target QM forces.

To parametrise the method for a new material, an initial dataset of relevant configurations (atomic positions and corresponding forces) is required. An appropriate set of IVs such as those in Eq. 6 must then be chosen, typically as the minimal set of vectors that carry good correlation with the target forces, i.e., lead to a low cross-validation error over the database. We envision that this process of optimal features selection could be automated with widely used techniques such as the LASSO method[38] outlined in Ref. 39. The input space descriptor used in our scheme is a 'feature matrix' $\mathbf{X} \in \mathbb{R}^{n_{\mathrm{IV}} \times n_{\mathrm{IV}}}$ constructed from the projection of all IVs onto the inner basis set $\{\hat{\mathbf{V}}_i = \mathbf{V}_i/|\mathbf{V}_i|\}$. This representation is used in a Gaussian kernel function

$$k(\mathbf{X}_i, \mathbf{X}_j) = \exp\left(-d(\mathbf{X}_i, \mathbf{X}_j)^2 / 2\sigma_{\mathrm{cov}}^2 \right) , \tag{7}$$

to construct the GP covariance matrix $\mathbf{C}$ will have entries

$$C_{ij} = k(\mathbf{X}_i, \mathbf{X}_j) + \sigma_{\mathrm{err}}^2 \delta_{ij} , \tag{8}$$

where $d(\mathbf{X}_i, \mathbf{X}_j)$ is an appropriately preconditioned Euclidean distance between teaching set configurations labelled i and j.[10] The correlation length scale σ_{cov} is optimised via a pre-

liminary cross-validation procedure over a sample dataset, while $\sigma_{\rm err}$ represents the nominal confidence interval of the calculated QM forces, here set to 0.05 eV/Å. The GP regression scheme operates in the internal vector space, so all forces are represented onto the over-complete $\{\hat{\mathbf{V}}_i\}$ basis set. For a configuration t, the posterior mean and variance of the force (y_t and σ_{y_t}, respectively) is calculated via the standard equations

$$y_t = \mathbf{k}^T \mathbf{C}^{-1} \mathbf{y}, \qquad \sigma_{y_t}^2 = \kappa - \mathbf{k}^T \mathbf{C}^{-1} \mathbf{k} \tag{9}$$

where $\mathbf{k}$ is the vector of kernel distances of t with respect to all other teaching set entries, κ is the covariance of the test configuration with itself and $\mathbf{y}$ is the vector of training output data. Finally, to reconstruct a predicted force in Cartesian space an overdetermined linear system is solved via least squares solution.[10]

We note in passing that the representation used here can be naturally extended to multi-component systems by constructing IVs only between atoms with the same chemical species, and combining these to form an extended feature matrix with a block structure that reflects the presence of the different species. Preliminary results indicate that this approach ensures that ML force prediction remains accurate for SiO_2 and SiC systems using similar, if slightly larger, database sizes (for full details cf. Ref. 10, Supplementary Material). Furthermore, our approach is also straightforwardly applicable to learn from higher-level quantum chemistry approaches. Namely, forces obtained from higher level schemes can be fed to the database in exactly the same way as DFT ones. An interesting scenario would arise in systems for which DFT and higher level (e.g., Quantum Monte Carlo, coupled cluster, etc.) forces were to be found substantially equivalent in many configuration space regions (e.g., close to structural minima corresponding to stable or metastable phases), but significantly different only in specific circumstances (e.g., for level-crossing configurations in molecular systems). If the relevant 'discrepancy' phase space regions were reasonably precisely identified in some well-controlled example system, a hybrid ML database could be constructed and grown in our scheme by computing the relatively affordable DFT forces where these are correct, and the expensive higher level forces only when needed: that is, just for the configurations where these are expected to differ significantly from the DFT ones. We speculate that such an approach could achieve an optimal mix of the two levels of theory, much in the general spirit

of the works by Refs. 40, 41.

Validation of the Force Learning Scheme

Systematic validation of our ML force calculation scheme has been carried out for crystalline and molten silicon model systems.[10] We find that converged prediction accuracy is typically achievable using only a few hundred most relevant data points selected from the full database. This is illustrated by Fig. 7, which includes a comparison with the predictions obtained using a teaching database chosen randomly from a large database. Clearly, searching for and selecting the most relevant data configurations for each new test configuration is preferable, and is thus used throughout the scheme. By using a fixed-size 'closer configurations' subsets also ensures that the overall computational cost of ML-predicting the force on an atom (of the order of 10^{-1} CPU-seconds in our tests) scales linearly with the database size. To appreciate the efficiency gain associated with the ML method, calculating the same force *ex novo* with a first principles method would typically require at least $\sim 10^2$ CPU-seconds.

To perform the ML on-the-fly, we combine the predicted ML forces with the LOTF predictor-corrector algorithm. We adjust the length of the predictor-corrector cycle, and hence the required frequency of QM calculations, in response to the force errors measured at each corrector stage. Our results for Si suggest that using ML allows the extrapolation length to be increased by at least a factor of three compared to the previous approach based on fitting to a fixed functional form at each QM force evaluation step.[5,10] Along an MD trajectory, we find that concentrated QM training is necessary at times when more chemical novelty is encountered, while fewer or no further QM calculations are needed if the system visits configuration space regions that have already been visited, and to the extent that they have effectively been learned. For relatively simple systems, such as low temperature ones, a sufficiently complete database can be obtained after a limited initial period of training, after which further QM calculation are just very occasionally needed to predict forces in the accessible portions of phase space. Fig. 8 shows results from simulations performed on Si at 1000 K using density functional tight binding[42] forces as the QM target. This calculation was carried out by monitoring the real error associated with the ML-predicted forces, compared with the target QM forces calculated at the predictor cycle endpoint. Two different force

error thresholds were selected to decide when to add additional QM information to the database. For the larger error threshold, QM training only happens during the first 2 ps and no further QM calls are needed, while at a tighter accuracy threshold occasional QM calls are still necessary after 7 ps. A stable predictor-corrector cycle length of 30 fs (i.e. a QM call frequency of 1/30 using a standard 1 fs time step for the dynamics) can be reached after 7 ps of simulations, demonstrating the capability of the new approach to accelerate first principles MD simulations. We note that monitoring predictor-stage actual force errors is a safe criterion, since this lifts the need for error estimations. Moreover, the MD trajectory is eventually integrated via ML-forces generated along the corrector stride, which by construction connects two system configurations well represented by the ML database, so that the ML force errors are significantly reduced.

OUTLOOK

In this work we have addressed two recent technical developments aimed at enabling efficient force-based QM/MM simulations on large HPC resources. First, we presented an ensemble parallelisation approach to split large individual QM calculations into several manageable portions. We then outlined a novel machine learning scheme that strives to predict, rather than recalculate, QM forces when encountering atomic configurations similar to those previously seen. In this section we discuss some implications of these two techniques, and suggest ways in which they could be combined to improve the information efficiency of simulating large atomistic systems. In our previous discussion of the ensemble parallelism scheme, the compute node allocation was filled by setting the total number k of QM subregions to $k = 2^N - 1$. This assumes that HPC partitions composed of 2^N blocks are allocatable through the queueing system, so k is chosen to keep one block free for non-QM work. However, once the constraint of running the same tasks on all blocks is removed, the flexibility of our partitioning scheme could be exploited more comprehensively. Namely, it would be straightforward to choose a smaller k value for the QM zone partitioning and fill up the additional free $n = 2^N - 1 - k$ compute node blocks with *any* other tasks consistent with improving the overall algorithmic efficiency (an example already encountered is splitting outlier

clusters of significantly larger than average dimensions after the partitioning and buffering phases). In particular, more QM cluster calculations could be performed to provide additional QM information where needed. As anticipated in the introduction, an unavoidable consequence of simulating large QM zones of *a priori* unpredictable chemical behaviour is that 'new' chemical events could occur in any set of localised QM subregions during the dynamical evolution of the system. In any such region the ML-predicted forces are by definition less reliable and the local frequency of necessary QM calculations must correspondently grow. An accuracy increase could be easily achieved by shortening the general predictor-corrector stride of the LOTF scheme. This would be inefficient, as QM calculations would then time-densify throughout the QM zone, even where this was not needed.

A much better strategy would consist of augmenting the ML database intake rate limited to the more 'difficult' QM subregions, where asynchronous supplementary QM calculations would be carried out. This way, any critical subregion experiencing a higher rate of chemical novelty would be allocated QM computations occurring at a commensurately higher rate. Such 'preconditioning' of the ML database growth rate over the QM zone would in turn allow using a unique, optimally large predictor-corrector stride throughout the system, while fresh QM information would be effectively computed in a fully importance-sampled way, in both the space and time domains. In a simple implementation, carrying out extra calculations at half the extrapolation length for a set of the n most critical QM subregions would provide new QM information for these at twice the normal frequency without compromising the load-balancing characteristics of the algorithm. A simple heuristic to identify the critical subregions would be to choose those for which the predictor force errors measured at the most recent QM force calculation are larger. The results of the additional half length predictor QM calculations would just be added to the ML database, to improve the accuracy of the following corrector stage and any ML-inferred forces from this point on.

To summarise, the procedure outlined above would combine ML force prediction with the ability of carrying out QM calculations on small selected system QM zone subregions. In particular, QM zone partitioning would make it possible to lift the predictor-corrector algorithm standard constraint of carrying out accurate calculations at the same fixed times everywhere in the QM zone. This would be accomplished without compromising the inter-

polation properties of the corrector loop, thus leaving unaffected the robustness of the LOTF scheme (the general idea is, however, implementation independent, as any learning QM/MM scheme could consider using partitioning to minimise QM calculations). We speculate that in many situations this would enable a significantly more efficient usage of the available HPC resources.

We finally note that carrying out additional QM calculations as suggested here would be expected to decrease, rather than increase, the overall ML database growth rate per unit simulated system time, compared with the synchronous scheme of Ref. 10 used with a shorter predictor-corrector stride. However, in either running modality the databases associated with ML methods are expected to grow large very quickly during the system evolution, and could be very large from start when incorporating QM data from previous simulations for similar systems. For this reason, we envisage that specific ('big data') techniques will eventually be needed to effectively deal with databases containing millions of configurations. For instance, a hierarchical clustering approach could be used to build a 'social network' encapsulating the dendrographic relationship between teaching data to identify the principal nodes of the network of configurations.

ACKNOWLEDGEMENTS

This work was funded by the Engineering and Physical Sciences Research Council under grant numbers EP/L014742/1 and EP/L027682/1. Additional financial support was provided by Argonne National Laboratory through a collaboration with the Thomas Young Centre and by the Rio Tinto Centre for Advanced Mineral Recovery based at Imperial College London. An award of computer time was provided by the Innovative and Novel Computational Impact on Theory and Experiment (INCITE) program. This research used resources of the Argonne Leadership Computing Facility, which is a DOE Office of Science User Facility supported under Contract DE-AC02-06CH11357.

References

1. J. R. Kermode, G. Peralta, Z. Li, and A. De Vita, Procedia Materials Science **3**, 1681 (2014).

2. M. Ciccotti, J. Phys. D Appl. Phys. **42**, 214006 (2009).

3. J. R. Kermode, T. Albaret, D. Sherman, N. Bernstein, P. Gumbsch, M. C. Payne, G. Csányi, and A. D. Vita, Nature **455**, 1224 (2008).

4. J. Song and W. Curtin, Nat. Mater. **12**, 145 (2013).

5. N. Bernstein, J. R. Kermode, and G. Csányi, Rep. Prog. Phys. **72**, 026501 (2009).

6. G. Kresse and J. Hafner, Phys. Rev. B **47**, 558 (1993).

7. S. J. Clark, M. D. Segall, C. J. Pickard, P. J. Hasnip, M. I. J. Probert, K. Refson, and M. C. Payne, Zeitschrift für Kristallographie **220** (2005).

8. J. Behler and M. Parrinello, Phys. Rev. Lett. **98**, 146401 (2007).

9. A. P. Bartók, M. C. Payne, R. Kondor, and G. Csányi, Phys. Rev. Lett. **104** (2010).

10. Z. Li, J. R. Kermode, and A. De Vita, Phys. Rev. Lett. **114**, 096405 (2015).

11. V. Botu and R. Ramprasad, Int. J. Quantum Chem. (2014).

12. C.-K. Skylaris, P. D. Haynes, A. A. Mostofi, and M. C. Payne, J. Chem. Phys. **122**, 084119 (2005).

13. J. M. Soler, E. Artacho, J. D. Gale, A. García, J. Junquera, P. Ordejón, and D. Sánchez-Portal, J. Phys.-Condens. Mat. **14**, 2745 (2002).

14. G. Csányi, T. Albaret, M. Payne, and A. De Vita, Phys. Rev. Lett. **93**, 175503 (2004).

15. G. Csányi, G. Moras, J. R. Kermode, M. C. Payne, A. Mainwood, and A. D. Vita, in *Topics in Applied Physics* (Springer Science + Business Media, 2006), pp. 193–212.

16. G. Csányi, S. Winfield, J. R. Kermode, A. De Vita, A. Comisso, N. Bernstein, and M. C. Payne, *Expressive programming for computational physics in fortran 95+* (2007), URL `https://camtools.cam.ac.uk/access/content/group/5b59f819-0806-4a4d-0046-bcad6b9ac70f/IoP_libatoms.pdf`.

17. J. VandeVondele, M. Krack, F. Mohamed, M. Parrinello, T. Chassaing, and J. Hutter, Comput. Phys. Commun. **167**, 103 (2005).

18. W. Kohn, Phys. Rev. Lett. **76**, 3168 (1996).

19. A. Peguiron, L. Colombi Ciacchi, A. De Vita, J. Kermode, and G. Moras, J. Chem. Phys. **142**, 064116 (2015).

20. J. Kermode, L. Ben-Bashat, F. Atrash, J. Cilliers, D. Sherman, and A. D. Vita, Nat. Comms. **4** (2013).

21. G. Moras, L. C. Ciacchi, C. Elsässer, P. Gumbsch, and A. De Vita, Phys. Rev. Lett. **105**, 075502 (2010).

22. A. Gleizer, G. Peralta, J. R. Kermode, A. De Vita, and D. Sherman, Phys. Rev. Lett. **112**, 115501 (2014).

23. J. R. Kermode and M. Caccin, *libAtoms/gepsipy package*.

24. B. Kernighan and S. Lin, Bell Syst. Tech. J. (1970).

25. C. Fiduccia and R. Mattheyses, Des. Autom. 1982. 19th Conference on. IEEE pp. 175–181 (1982).

26. D. Spielmat, in *Proc. 37th Conf. Found. Comput. Sci.* (IEEE Comput. Soc. Press, 1996), pp. 96–105.

27. A. Pothen, H. D. Simon, and K.-P. Liou, SIAM J. Matrix Anal. Appl. **11**, 430 (1990).

28. G. Karypis and V. Kumar, SIAM J. Sci. Comput. **20**, 359 (1998).

29. A. A. Hagberg, D. A. Schult, and P. J. Swart, in *Proceedings of the 7th Python in Science Conferences (SciPy 2008)* (2008), vol. 2008, pp. 11–16.

30. J. E. Gentle, L. Kaufman, and P. J. Rousseuw, Biometrics **47**, 788 (1991).

31. M. Fiedler, Czechoslov. Math. J. **23** (1973).

32. M. Fiedler, Czechoslov. Math. J. **25** (1975).

33. D. Lee, S. Park, J. Lee, and N. Hwang, Acta Mater. **55**, 5281 (2007).

34. R. A. Haring, M. Ohmacht, T. W. Fox, M. K. Gschwind, D. L. Satterfield, K. Sugavanam, P. W. Coteus, P. Heidelberger, M. A. Blumrich, R. W. Wisniewski, et al., Micro, IEEE **32**, 48 (2012).

35. D. MacKay, *Information theory, inference and learning algorithms* (Cambridge Univ Press, Cambridge, 2003).

36. F. H. Stillinger and T. A. Weber, Phys. Rev. B **31**, 5262 (1985).

37. J. R. Kermode, S. Cereda, P. Tangney, and A. De Vita, J. Chem. Phys. **133**, 094102 (2010).

38. R. Tibshirani, J. R. Stat. Soc. Ser. B Stat. Methodol. pp. 267–288 (1996).

39. L. M. Ghiringhelli, J. Vybiral, S. V. Levchenko, C. Draxl, and M. Scheffler, Phys. Rev. Lett. **114**, 105503 (2015).

40. J. Grossman and L. Mitas, Phys. Rev. Lett. **94**, 056403 (2005).

41. A. P. Bartók, M. J. Gillan, F. R. Manby, and G. Csányi, Phys. Rev. B **88**, 054104 (2013).

42. M. Elstner, D. Porezag, G. Jungnickel, J. Elsner, M. Haugk, T. Frauenheim, S. Suhai, and G. Seifert, Phys. Rev. B **58**, 7260 (1998).

Figure 1: Tiling options for running a QM/MM calculation on a 16-block job partition: each small square corresponds to one block, and an executable can only run on 2^N blocks. (a) The allocation is only partially occupied; (b) The allocation fully occupied, but the MD partition is unnecessarily large; (c) Optimal partition tiling enabled by the ensemble parallel QM calculations proposed in this work.

Figure 2: Example step of the digestive ripening algorithm on a connected graph comprising $k = 3$ subgraphs: (a) Initial partitioning; (b) Identification of the region i^* most dissimilar from the others (brown vertices/atoms) and its neighbour vertices (in grey); (c) Calculation of gain for all possible moves (three arrows) and selection of the highest gain move (bold arrow); (d) Updated partitioning, where the k subgraphs are more commensurate and compact.

Figure 3: Benchmark system for weak scaling: crack tip of a-SiO_2. (a) Minimal size whole system for QM/MM simulation of SiO_2 glass fracture, comprising ~ 30000 atoms. (b) Crack tip closeup. The core QM region $\mathcal{C}$ is represented in red. Larger beads are Si atoms, smaller beads are O atoms. Here $|\mathcal{C}| = 218$ atoms. (c) $\mathcal{C}$ partitioned in $k = 15$ parts: each connected set of equally coloured atoms corresponds to a different $\mathcal{C}_i$ (PBCs apply). $|\mathcal{C}_i| = 15$ atoms on average. (d) Example of a cluster $\mathcal{C}_i \cup \mathcal{B}_i$ sent for DFT calculation. C atoms are represented in red, buffer atoms are white. The cluster contains $|\mathcal{C}_i \cup \mathcal{B}_i| \sim 250$ atoms.

Figure 4: Correlation between cost function of each as-partitioned core QM subregion $\mathcal{C}_i$ and the number of valence electrons of core and buffer region of the atomic cluster used to calculate forces in $\mathcal{C}_i$. The system is the a-SiO_2 crack tip used for the weak scaling benchmark (cf. Fig. 3). Results are shown for 3 systems comprising a different number of total core QM atoms $|\mathcal{C}|$ and corresponding number of partitions of the QM zone k.

Figure 5: Weak scaling of the ensemble parallel method: the time to solution is given as a function of the problem size, here the number $|\mathcal{C}|$ of atoms in the full core QM region. For the ensemble method (green circles), the ratio between the number of core QM atoms and the number of compute nodes (CNs) for the total calculation is kept approximately fixed: problem sizes of $|\mathcal{C}| = 218, 436, 872$ atoms correspond to splitting the full QM region in $k = 7, 15, 31$ parts, respectively. The total CNs assigned to the DFT calculations are given by $N_{\mathrm{DFT}} = 64 \cdot k$, corresponding to a concurrent use of 448, 960, and 1984 CNs. The cost of a single CP2K calculation for the 218 and 436 atom systems using $N_{\mathrm{DFT}} = 512$ and 1024 nodes, respectively, is shown for comparison (orange triangles). Ideal scaling would correspond to a constant time to solution.

Figure 6: Strong scaling of ensemble parallel method: the total computational cost — measured as the wall-clock time taken by the calculation times the total number N_{DFT} of compute nodes used — is shown as a function of the total number of compute nodes assigned to DFT calculations N_{DFT}. The core QM region (here, a Si crack tip) is kept constant, and the ensemble results (green circles) are shown for partitionings into $k = 1, 3, 7, 15$ parts respectively, corresponding to a concurrent use of $N_{\mathrm{DFT}} = 64 \cdot k$ compute nodes. For a comparison with a single DFT calculation on the whole QM zone using the same DFT code, the results are shown for $N_{\mathrm{DFT}} = 64$, 256, and 512 compute nodes (orange triangles). Ideal scaling would correspond to constant computational cost (blue solid line).

Figure 7: Accuracy of ML force predictions for bulk Si at 1000 K as a function of the teaching database size. The teaching set of size N_{teach} is extracted from a larger database either randomly (orange triangles) or by selecting the configurations nearest to the one for which force prediction in needed (green circles). Convergence is more rapidly achieved when the most relevant data are selected, and in both cases the force error converges to an acceptable threshold accuracy of ~ 0.1 eV/Å.

Figure 8: Running average rate of fresh QM force calculations necessary to guarantee that errors of the ML force prediction do not exceed a given threshold, here set to 0.15 eV/Å (yellow) and 0.2 eV/Å (blue). The dashed horizontal line represents the QM rate in the case of a constant 30 fs predictor-corrector stride.

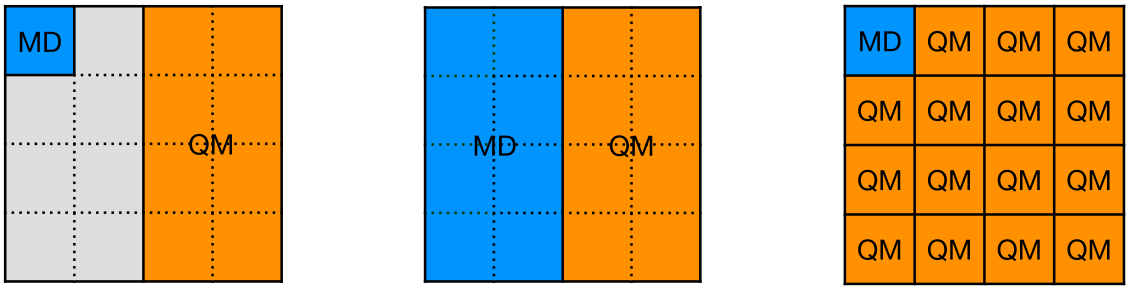

Figure 1
Marco Caccin, Zhenwei Li, James R. Kermode, Alessandro De Vita
Int. J. Quant. Chem.

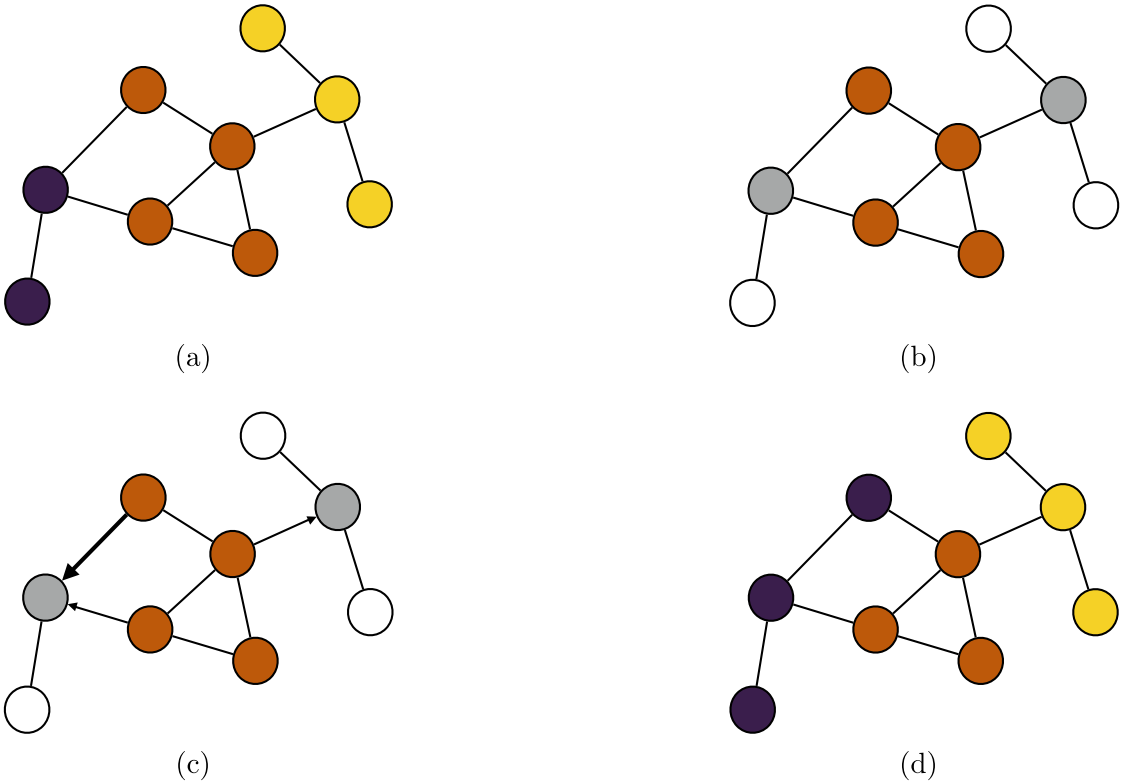

Figure 2
Marco Caccin, Zhenwei Li, James R. Kermode, Alessandro De Vita
Int. J. Quant. Chem.

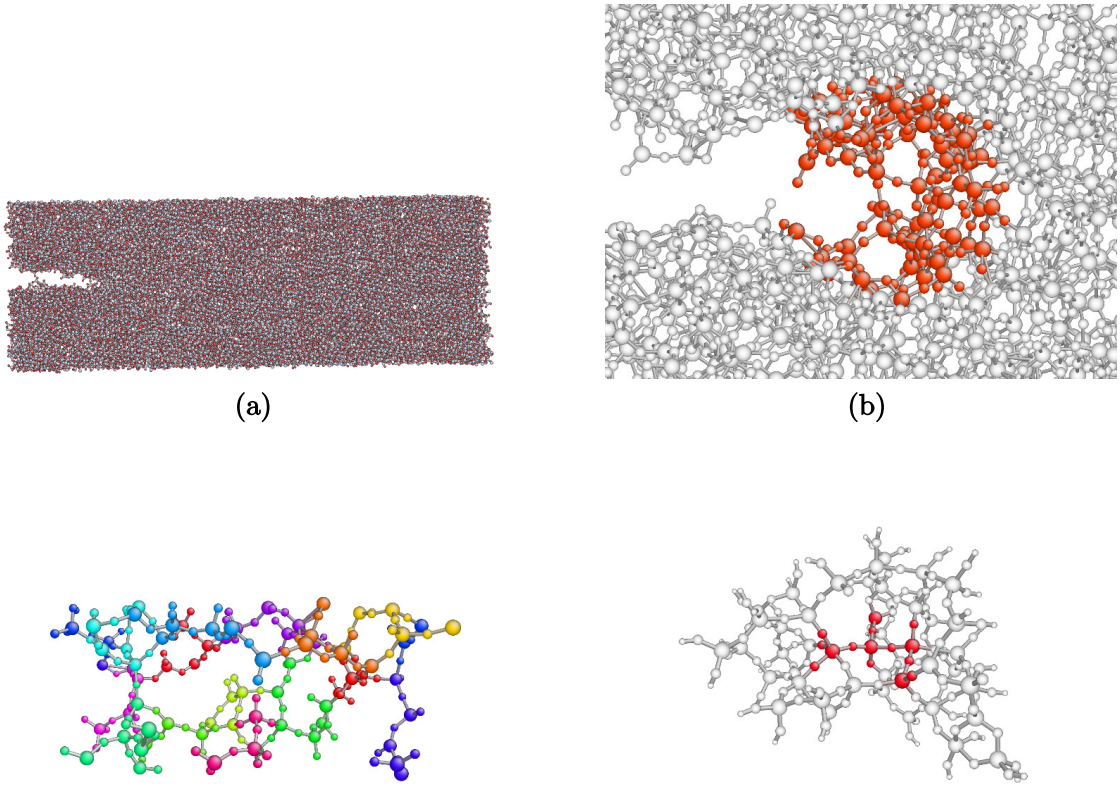

(a) (b) (c) (d)

Figure 3
Marco Caccin, Zhenwei Li, James R. Kermode, Alessandro De Vita
Int. J. Quant. Chem.

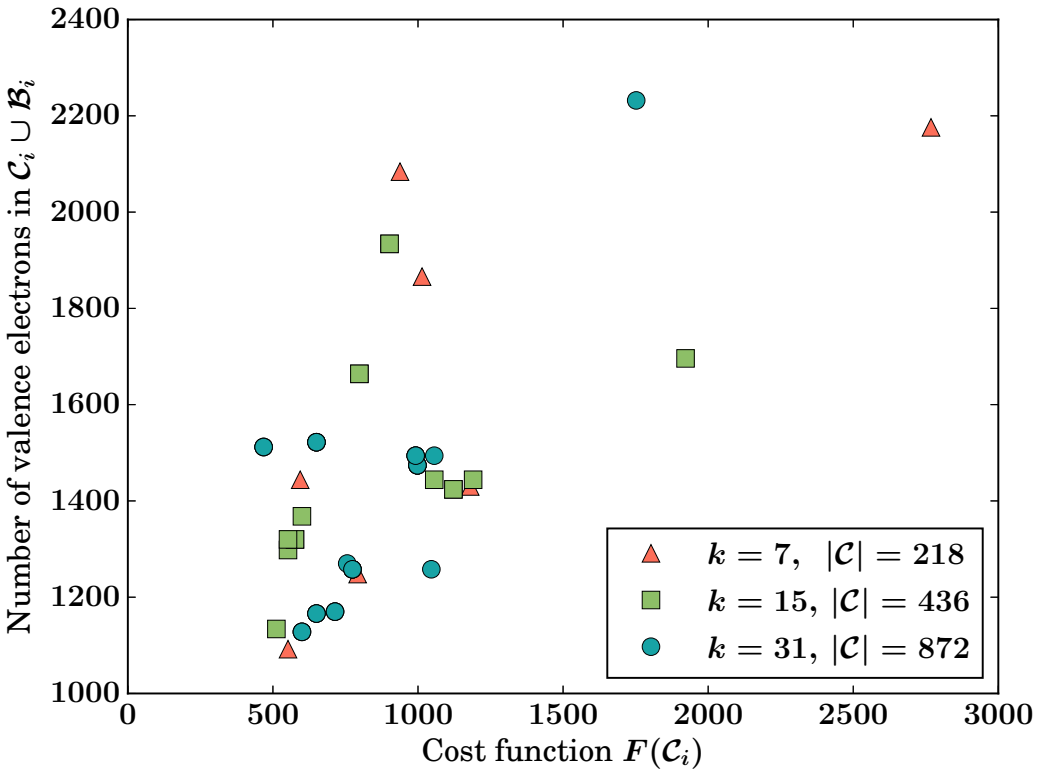

Figure 4
Marco Caccin, Zhenwei Li, James R. Kermode, Alessandro De Vita
Int. J. Quant. Chem.

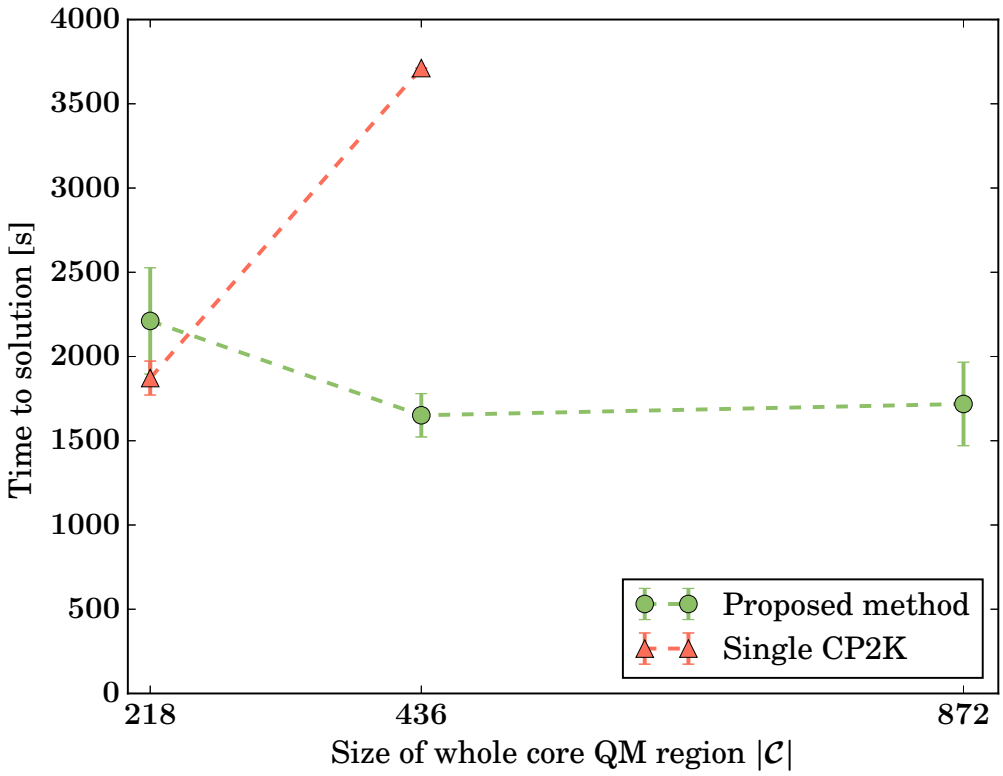

Figure 5
Marco Caccin, Zhenwei Li, James R. Kermode, Alessandro De Vita
Int. J. Quant. Chem.

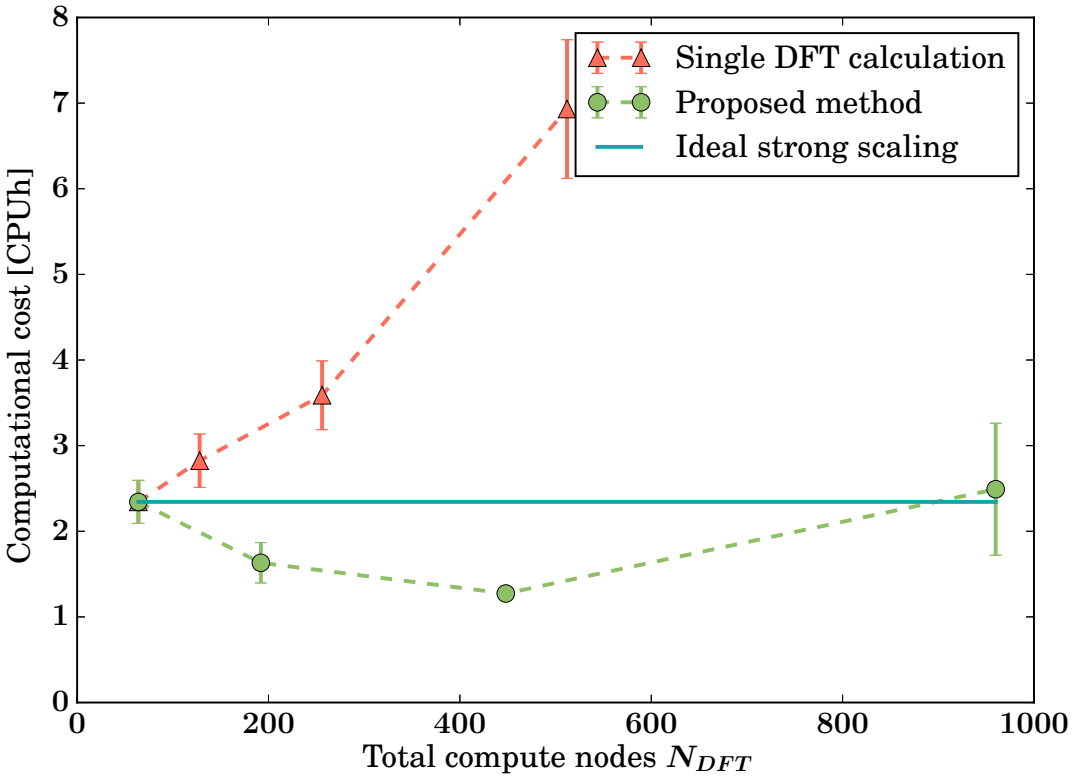

Figure 6
Marco Caccin, Zhenwei Li, James R. Kermode, Alessandro De Vita
Int. J. Quant. Chem.

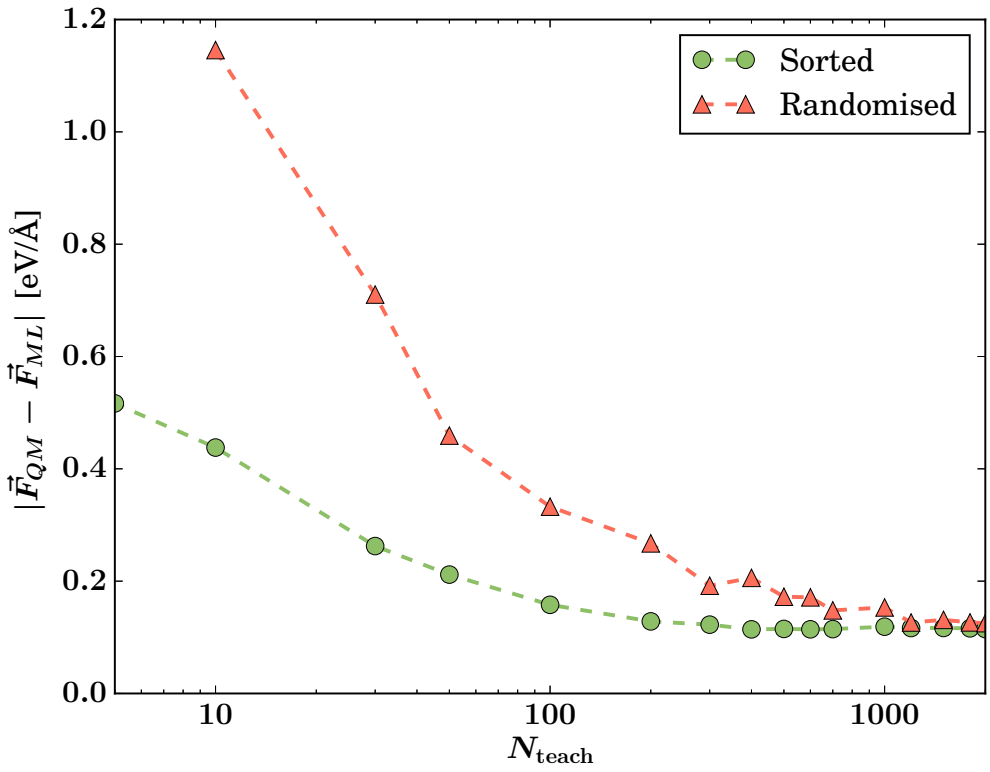

Figure 7
Marco Caccin, Zhenwei Li, James R. Kermode, Alessandro De Vita
Int. J. Quant. Chem.

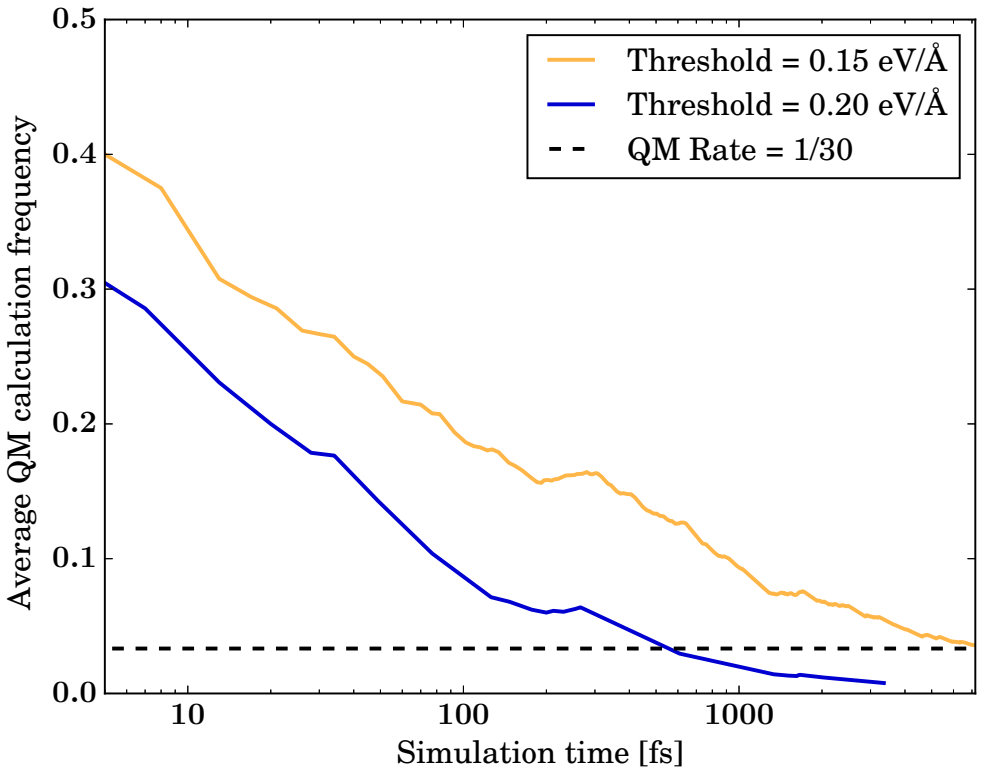

Figure 8
Marco Caccin, Zhenwei Li, James R. Kermode, Alessandro De Vita
Int. J. Quant. Chem.